Chemistry Europe
European Chemical Societies Publishing

WILEY VCH

Excellence in Chemistry Research

Announcing our new flagship journal

- Gold Open Access
- Publishing charges waived
- Preprints welcome
- Edited by active scientists

Meet the Editors of *ChemistryEurope*

Luisa De Cola
Università degli Studi di Milano Statale, Italy

Ive Hermans
University of Wisconsin-Madison, USA

Ken Tanaka
Tokyo Institute of Technology, Japan

ChemistrySelect

Research Article
doi.org/10.1002/slct.202202879

Chemistry Europe
European Chemical Societies Publishing

www.chemistryselect.org

Highly-Dispersed Vanadium Nitride Supported on Porous Nitrogen-Doped Carbon Material as a High-Performance Cathode for Lithium-Sulfur Batteries

Li Wang,[a] Chaoyang Sun,*[b] Shan Ji,*[c] Vladimir Linkov,[d] and Hui Wang*[b]

Transition metals and their compounds supported on carbon materials are widely used as cathodes for lithium-sulfur batteries. Vanadium nitride is considered to be a promising cathode because of its good adsorption capacity for lithium polysulfides and high catalytic activity, but in practice it usually shows insufficient electrical conductivity and low electrocatalytic activity due to particles agglomeration. In this study, highly dispersed vanadium nitride supported on porous nitrogen-doped carbon was prepared via one-pot pyrolysis in a molten salt medium. Physical characterization revealed VN particles with a uniform size distribution of ca. 10 nm well dispersed on the carbon surface. When used as a cathode for Li–S battery, the material delivered a specific discharge capacity of 1050 mAh g^{-1} at 0.2 C and good rate performance. During the stability test over 500 continuous cycles, the average decay rate was 0.059% per cycle. The study demonstrates prospective application of the newly developed electrocatalytic material as a cathode in lithium-sulfur batteries.

Introduction

Lithium-sulfur batteries are considered to be the most promising new secondary batteries due to their high theoretical specific capacity of 1675 mAh g^{-1}, much higher than those of conventional Li-ion cells.[1,2] However, low electrical conductivities of S and Li_2S compounds and the shuttle effect of soluble lithium pholysulfides significantly impede their practical applications in energy storage devices.[3,4] Significant research effort has been dedicated to resolve these problems, mainly focusing on developing new cathodes containing alternative sulfur hosts, such as porous carbons,[4,5] graphene[6,7] and conductive polymers.[8,9] Porous carbons attracted much research attention due to their high electrical conductivity and the possibility to physically confine active materials in the well-developed porous structure with large surface area allowing for further modifications to enhance electrocatalytic performance.[10–12]

Vanadium nitride (VN)[13,14] has been widely used as a cathode material for lithium-sulfur batteries due to its high catalytic activity and significant adsorption capacity for polysulfides.[15–17] However, poor dispersion of VN results in low catalytic activity, which limits its practical application. The combination of VN with porous carbons is expected to solve this problem.

It was recently shown that highly conductive VN applied as a carbon-free electrode can achieve uniform nucleation of Li and suppress the growth of Li dendrites, which accelerates the conversion of polysulfides.[18–20] For instance, Manthiram *et al.* prepared 3D aerogels composed of vanadium nitride nanowires as electrode materials able to capture polysulfides, as was confirmed by UV-Vis absorption spectroscopy,[15] which demonstrated high catalytic activity in polysulfide conversion. However, the application of pure VN leads to low sulfur loading and significant loss of the active material during cycling, due to its low specific surface area. To solve this problem, VN was deposited onto carbon materials possessing large specific surface areas. Yu *et al.*[21] successfully loaded VN quantum dots on graphene substrates by means of hydrogen peroxide assisted hydrothermal reaction and gradient nitridation, to yield the material with an enhanced catalytic activity. However, due to the small specific surface area of the support, VN quantum dots could not provide sufficient active sites, which calls for selecting carbon substrates with higher surface areas. As a successful cathode material for lithium-sulfur batteries, well dispersed VN will effectively adsorb lithium polysulfides, to slow down the shuttle effect, in combination with its inherently high redox catalytic activity.[22]

According to previous studies, a support with high specific surface area containing uniformly dispersed VN particles will result in a high performance stable electrode. In this work, VN was uniformly supported within the porous N-doped carbon network by one-step carbonization in a molten salt medium, where peptone was used as a carbon and nitrogen source, NaCl as a molten salt template and NH_4VO_3 as a vanadium source. Using this method, VN could be easily, uniformly and

[a] *L. Wang*
School of Chemistry & Environmental Engineering, Pingdingshan University,
Pingdingshan 467000, China
[b] *C. Sun, H. Wang*
State Key Laboratory Base for Eco-Chemical Engineering, College of Chemical Engineering, Qingdao University of Science and Technology, Qingdao, 266042, China
E-mail: 1589668821@qq.com
wangh@qust.edu.cn
[c] *S. Ji*
College of Biological, Chemical Science and Engineering, Jiaxing University, Jiaxing, 314001, China
E-mail: shan.ji@ucl.ac.uk
[d] *V. Linkov*
South African Institute for Advanced Materials Chemistry, University of the Western Cape, Cape Town, 7535, South Africa

Supporting information for this article is available on the WWW under https://doi.org/10.1002/slct.202202879

controllably deposited onto in situ formed porous N-doped carbon. VN nanoparticles with high catalytic activity were strongly physically adsorbed on porous nitrogen-doped carbon to produce the Li–S battery cathode with high initial specific discharge capacity and good cycling stability.

Experimental

Synthesis proceduresPreparation of VN@NC

1 g of peptone and 0.03 mmol of NH_4VO_3 were added to 10 mL of water and ultrasonicated for 30 min. The solution was frozen in liquid nitrogen and freeze-dried for 48 h. The dried sample was grinded into powder, which was mixed with 10 g of NaCl and ball-milled for 3 h. Subsequently, the sample was heated to 900 °C in a tube furnace at a rate of 5 °C/min and kept at this temperature for 1 h. The obtained sample was thoroughly washed by deionized water to remove NaCl, followed by drying in a vacuum oven at 60 °C for 12 h. The dried sample are labeled as VN@NC.

For comparison, two samples were prepared at the same temperature, one via two step carbonization (VN/NC) and another without the addition of vanadium (NC), according to the procedures described below. Chemicals used in the experiment, such as table1.

Preparation of VN/NC

1 g of peptone and 10 g of NaCl were mixed and ball-milled for 3 h and carbonized at 900 °C for 1 h after heating to this temperature at a rate of 5 °C/min. NaCl in the obtained sample was removed by washing with deionized water. 100 mg of the sample was added to 10 mL of aqueous solution containing 10 mg of NH_4VO_3. Subsequently, the solution was dried by rotary evaporation to obtain a black powder, which was placed into a tube furnace and heated to 900 °C at a rate of 5 °C/min, followed by carbonization for 1 h. The cooled sample was rinsed with water and dried in a vacuum oven at 60 °C for 12 h. The dried sample was labeled as VN/NC.

Preparation of NC

1 g of peptone and 10 g of NaCl were mixed and ball-milled for 3 h, heated to 900 °C at a rate of 5 °C/min and carbonized for 1 h. The sample was rinsed thoroughly with deionized water and dried in a vacuum oven at 60 °C for 12 h. The dried sample was labelled as NC.

Results and discussion

The synthesis procedure of VN@NC is schematically shown in Figure 1. In this method, peptone was selected as a C and N source to form N-doped carbon. Peptone and NH_4VO_3 were dissolved in 10 mL of deionized water and freeze-dried. The sample was ball-milled with NaCl, a template to form the porous structure and heated at 900 °C for 1 h.[23,24] NaCl melted at the high temperature and formed nanodroplets, which can penetrate the N-doped carbon precursor during the carbonizing process, leading to the formation of porous structure in the resulting material. Simultaneously, vanadium nitride was formed on the surface of N-doped carbon via the pyrolysis of NH_4VO_3 according to the following equations(1–3):

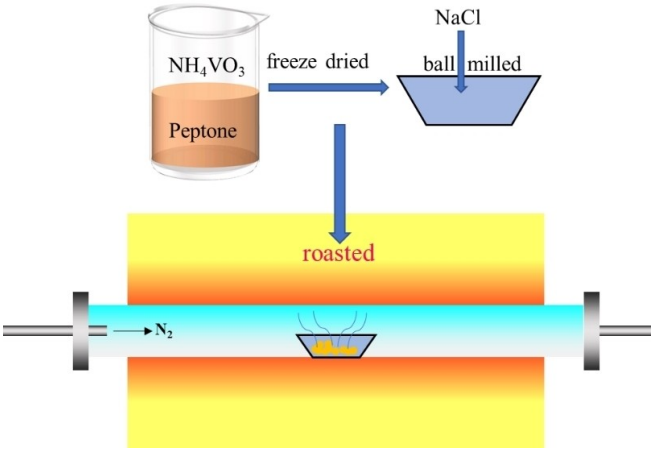

Figure 1. Schematic diagram of VN@NC synthesis.

$$2NH_4VO_3 \rightarrow V_2O_5 + H_2O + 2NH_3 \quad (1)$$

$$V_2O_5 + NH_3 \rightarrow VN_xO_y + H_2O \quad (2)$$

$$VN_xO_y + NH_3 \rightarrow VN + H_2O \quad (3)$$

Subsequently, NaCl template was completely removed by rinsing in water. Compared to conventional hard-templating methods,[25] application of a molten salt template can significantly simplify the template removing procedure by washing with water.

The morphology and the microstructure of as-prepared samples were initially investigated by SEM. A porous structure without obvious particles was observed in SEM images of VN@NC (Figure 2a–2c). VN/NC also exhibited a porous network, but agglomerated metal particles were found on the surfaces as shown in Figures 2d–2f. No particles were found in the SEM image of NC (Figures 2g–2i), implying that agglomerated particles found on VN/NC resulted from the decomposition of NH_4VO_3. Images of three samples presented in Figure S1 confirm the formation of porous structure by molten NaCl with no visible pore destruction caused by the introduction of NH_4VO_3.

Figures 3a and S3 deal with XRD investigation of the crystallinity of the newly prepared materials, where the VN@NC diffraction peak at 26° corresponds to (002) plane of C,[26] and the peak at 43° - to (200) plane of VN,[27] indicating that the NV phase was successfully formed on carbon. The peak at 43° is not visible in the XRD pattern of NC, and the XRD pattern of VN/NC confirmed the formation of VN particles on VN/NC (Figure S3). According to Figure 3b, particle sizes of VN in VN@NC range from 8–15 nm. The presence of elements C, N, V and O was detected in VN@NC (Figure 3c).

TEM images of the porous structures presented in Figure 3d reveal thin carbon layers interconnected with each other, with VN particles covering layer surfaces (Figure 3e). Even distribution of embedded metal particles is visible in the TEM image shown in Figure 3f. According to Figure 3g, the particle fringes have a lattice spacing of 0.24 nm, corresponding to (200) plane

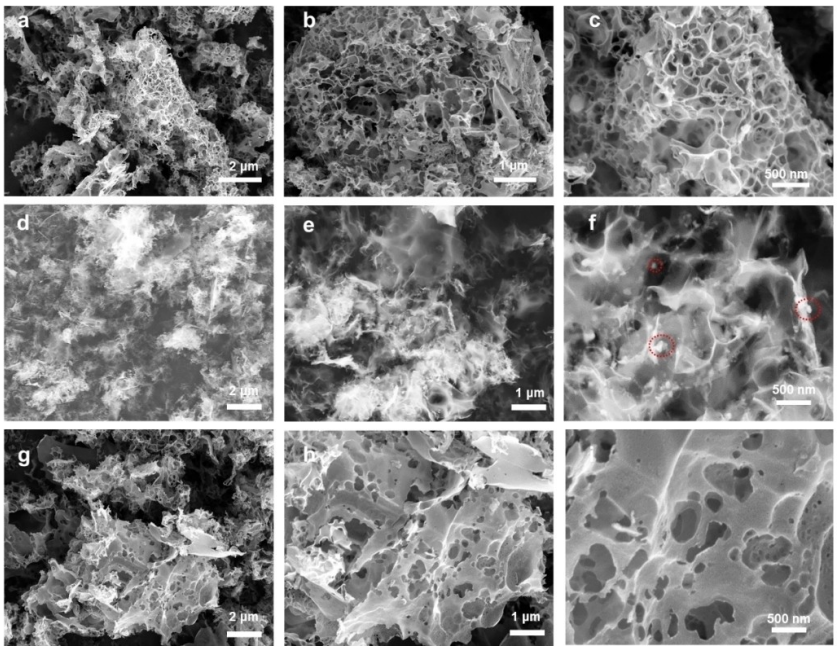

Figure 2. SEM images of (a–c) VN@NC, (d–f) VN/NC and (g–i) NC.

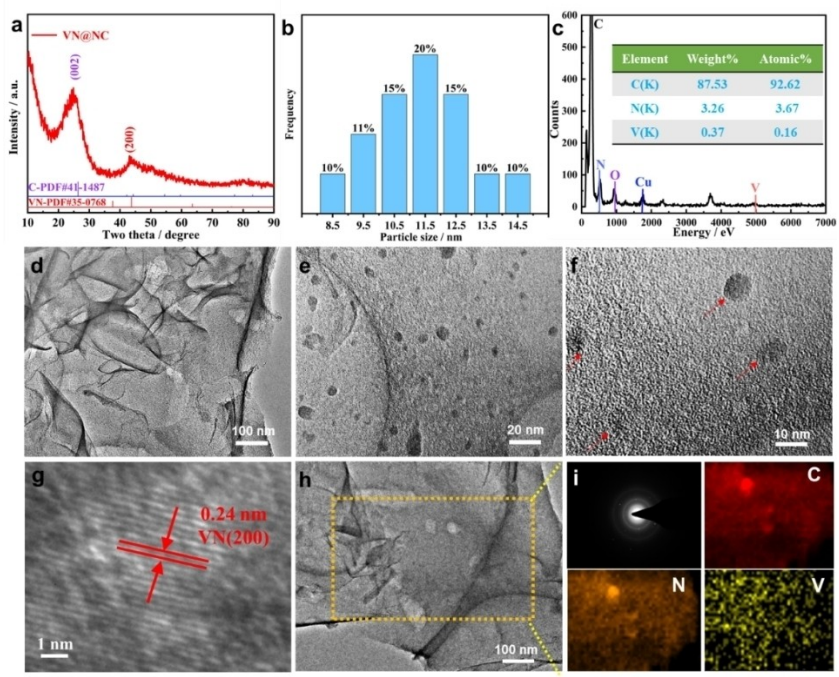

Figure 3. (a) XRD pattern, (b) particle size distribution, (c) EDS spectrum, (d–f) TEM images and (h–i) electron diffraction and elemental analysis of C, N, and V in VN@NC.

of VN.[28] Element mapping images shown in Figures 3h–3i testify to even distribution of C, N and V in carbon layers.

XPS spectra of VN@NC, shown in Figure 4a, reveal the presence of C, N, V, and O elements, the latter resulting from the long air exposure of the sample. High-resolution C 1s XPS spectrum contains four fitted peaks at 284.8, 385.6, 286.7, and 289.1 eV, corresponding to C–C, C–N, C–O and C=O bonds, respectively,[29] which proves successful doping of N into the carbon matrix (Figure 4b). The N 1s XPS signal was fitted into four peaks at 397.2, 398.5, 400.2, 401.0 and 403.2 eV, which were attributed to pyridinic N, pyrrolic N, V–N, graphitic N and pyridinic-N-oxide, respectively (Figure 4c).[30] N species in

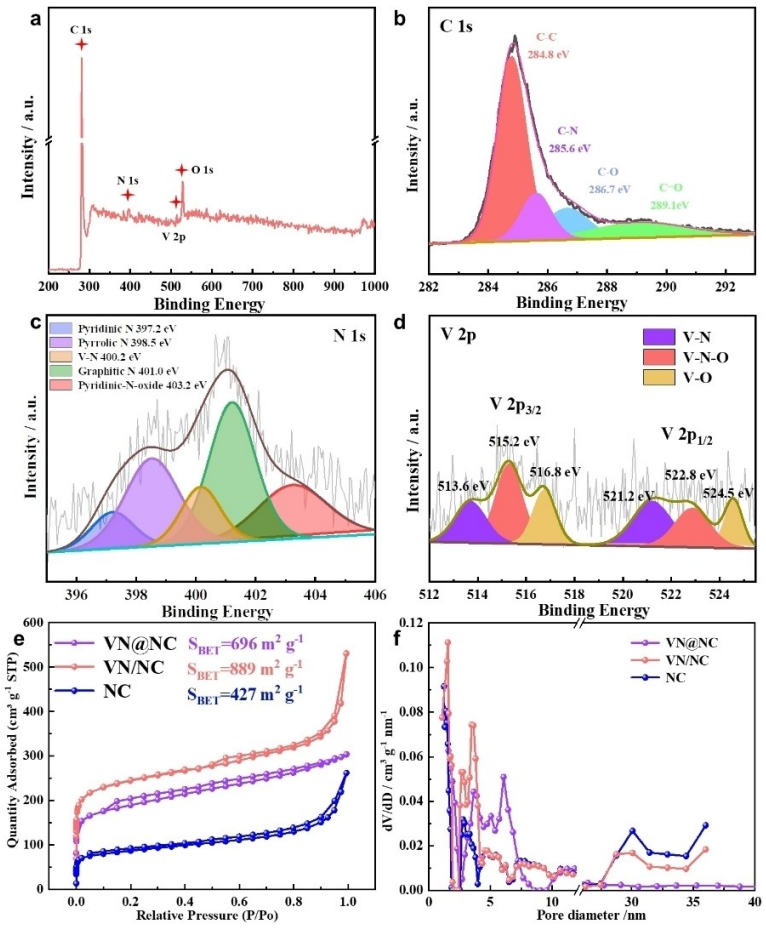

Figure 4. (a) XPS full spectrum, (b) C 1s, (c) N 1s (d) fine spectrum of V 2p, (e) nitrogen adsorption and desorption curves, (i) pore size distribution of VN@NC.

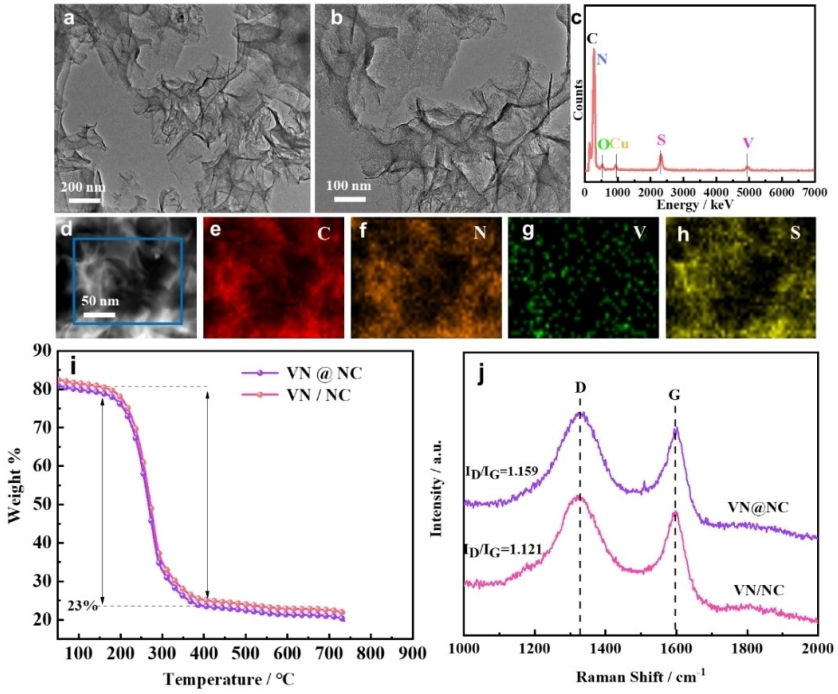

Figure 5. (a–b) TEM image, (c) EDS image and (d–h) elemental analysis of C, N, V, S in S@VN@NC. (i) TG curve, (j) Raman in VN@NC and VN/NC.

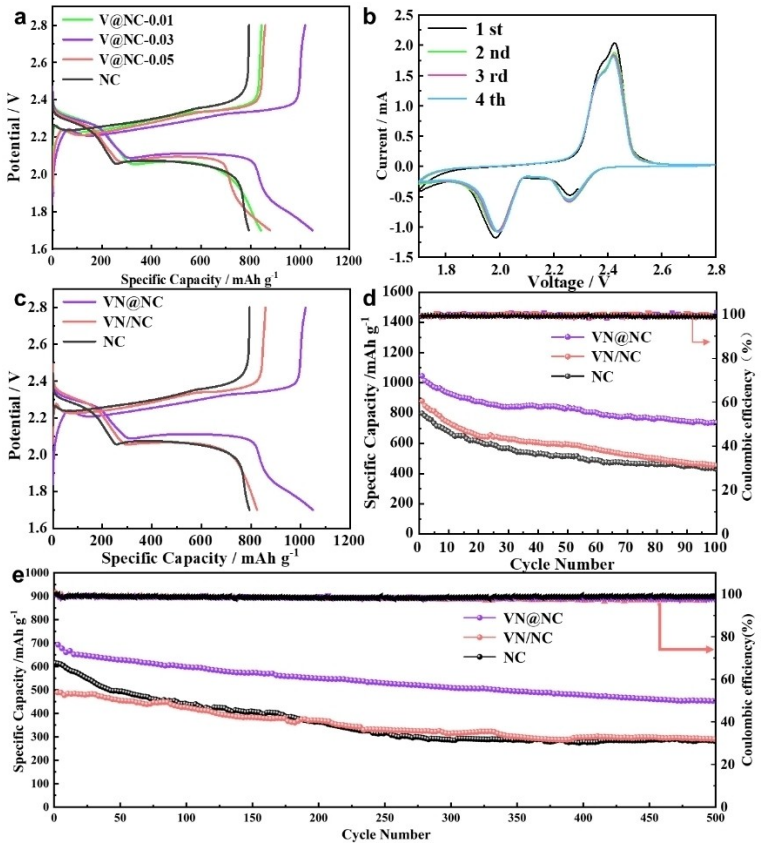

Figure 6. Charge and discharge curves of (a) S@VN@NC-0.01, S@VN@NC-0.03, S@VN@NC-0.05 and S@NC at 0.2 C, (b) cyclic voltammetry curves of S@VN@NC, (c) charge-discharge curves of S@VN@NC, S@VN/NC and S@NC at 0.2 C, (d) cycling stability at 0.2 C, (e) cycling stability at 1 C (Area load 2 mg cm^{-2}).

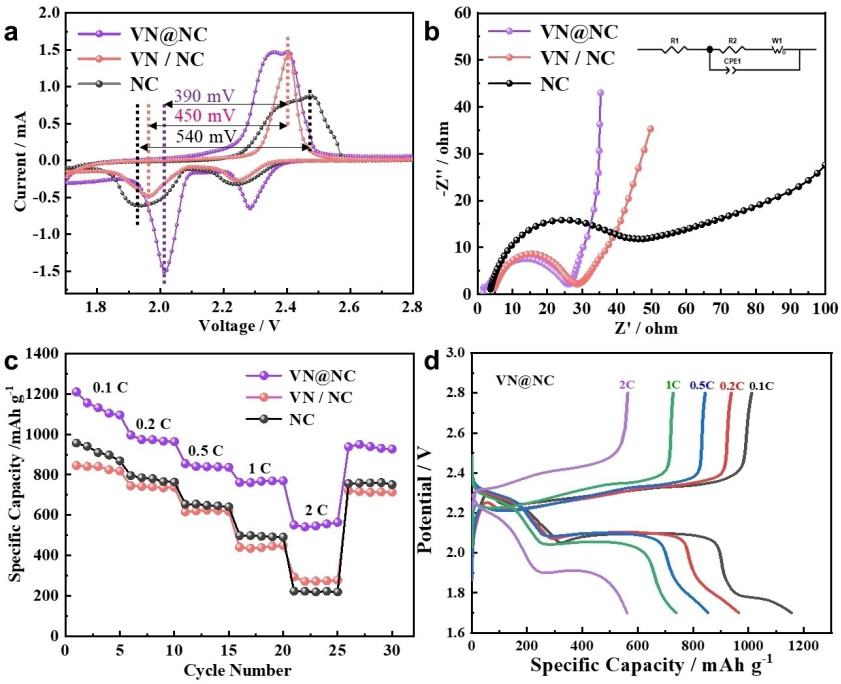

Figure 7. (a) Cyclic voltammograms of S@VN@NC, S@VN/NC and S@NC; (b) EIS; (c) rate performance; (d) discharge curves at various rates.

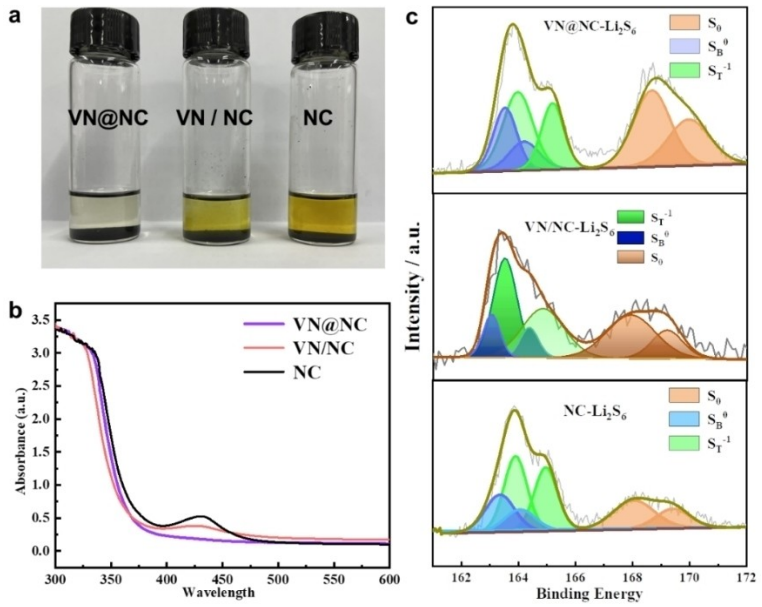

Figure 8. (a) Images of VN@NC, VN/NC and NC added to Li_2S_6 solutions for 0.5 h; (b) UV-vis absorption spectra; (c) fitted S 2p XPS after adsorption of Li_2S_6.

VN@NC are mainly composed of pyridine nitrogen and pyrrole nitrogen, which are considered to be adsorption sites for polysulfides.[31] The V–N bond was evident from N 1s XPS spectrum, further proving the presence of V in the nitride form. The fitted V 2p XPS spectrum of VN@NC is shown in Figure 4d, where the peaks at 515 and 523 eV correspond to V $2p_{3/2}$ and V $2p_{1/2}$ orbitals, respectively, and the peaks at 513.6 and 521.2 eV result from V–N bonds, further indicating the formation of VN.[32,33] The peaks at 515.2 and 522.8 eV were attributed to the V–N–O bond, and the peaks at 516.8 and 524.5 eV - to V–O bond, caused by air oxidation.[17]

Nitrogen isothermal adsorption/desorption curves, recorded to evaluate the porosity of the samples (Figure 4e), show a rapid uptake in the relatively low pressure region, due to a large number of micropores. The hysteresis loop appears in the medium pressure region, indicating the mesoporous structure. Calculated BET surface areas of VN@NC, VN/NC and NC were 696, 889 and 427 m^2/g, respectively, indicating an increase after the VN loading. This could result from the decomposition of NH_4NO_3, accompanied by the volume shrinkage and the formation of both micro- and mesopores, the latter providing more channels for electrolyte transfer, making more active sites available for electrocatalytic reactions.[34]

VN@NC, VN/NC and NC were ground with sublimed sulfur and heated at 155 °C to produce sulfur loaded materials labeled as S@VN@NC, S@VN/NC and S@NC, respectively. The condition of 155 °C is most conducive to sulfur diffusion into the carbon porous structure, due to minimal viscosity of sulfur at this temperature. The sulfur peak was detected in all XRD patterns (Figure S4), confirming successful loading. TEM images demonstrated original carbon layer structure and morphology in S@VN@NC, without sulfur particles or lumps, which, in conjunction with results presented in Figure 5c, testifies to successful sulfur loading. Uniform dispersion of C, N, V and S, with sulfur filling the pores of carbon porous structure, is evident from the element distribution images shown in Figures 5d–5f. The similarity of S dispersion pattern to those of C and N further confirms its uniform distribution within VN@NC. According to Figure S2, more particles are present on the surface of VN/NC than that of VN@NC, possibly due to abundant elemental sulfur adsorption sites in the latter, preventing pore blockages by excess sulfur. Figures S2b and S2c give more details of sulfur aggregation on the surface of VN/NC, which is not visible in the TEM images of NC. Presumably, sulfur aggregation on VN/NC resulted from VN particles present on its surface, due to their strong sulfur affinity, with larger VN particles blocking the penetration of sulfur into the porous carbon structure. By analyzing the TG curves of VN@NC and VN/NC, as shown in Figure 5i, the weight began to decrease at about 150°C, and finally stabilized at 23 %, which proved that the amount of metal added was basically the same. Further Raman test results are shown in Figure 5j. The higher peak value of ID/IG of VN @ NC indicates that there are more defects in the increase of disorder. This provides help for the subsequent catalytic conversion of lithium polysulfide.

The sulfur content of the sample tested by thermogravimetry is 70 % as shown in Figure S5. The sulfur-loaded (70 %) samples were used to assemble Li–S cells which electrochemical performance is presented in Figure 6. Initially, the effects of different VN loadings (0.01 mmol, 0.03 mmol and 0.05 mmol) were investigated using charge / discharge curves. As shown in Figures 7a and S6, S@VN@NC-0.03 had the highest initial specific discharge capacity and best cycling stability, which prompted the selection of this cell for further electro-

chemical tests. In all S@VN@NC cells, the first four CV cycles exhibited two pairs of overlapping redox peaks, indicating the reversible redox reaction.[35] According to Figure 6c, specific discharge capacity of the S@VN@NC cell reaches 1050 mAh g^{-1} at 0.2 C, much higher than those of S@VN/NC (815 mAh g^{-1}) and S@NC (798 mAh g^{-1}). This could result from the highly dispersed VN phase, which accelerates the conversion of polysulfides, making more sulfur available for electrochemical processes. During stability tests illustrated in Figure 6d, a capacity retention of 75% was recorded after 100 cycles at 0.2 C. At a high current density of 1 C, the cell still maintained high initial specific capacity and good cycling stability with a decay rate of only 0.059% per cycle for 500 cycles (Figure 6e). The latest performance comparison with vanadium-based carbon materials is shown in table S1.

CV curves of S@VN@NC, S@VN/NC and S@NC, shown in Figure 7a, have two pairs of redox peaks. The highest oxidation current observed for S@VN@NC indicates its good catalytic activity towards polysulfides. The oxidation peak appeared at 2.4 V, the corresponding reduction peak - at 2.01 V, with the potential difference of only 390 mV. The potential differences for other two materials were 450 and 540 mV, respectively, proving that VN@NC can promote redox of polysulfides with much faster kinetics. EIS results presented in Figure 7b demonstrate the lowest charge transfer resistance of S@VN@NC, represented by its smallest semicircle radius in the high frequency region. This proves that the combination of highly dispersed VN and porous N-doped carbon can accelerate charge transfer effectively. The straight line in the low frequency region represents diffusion resistance, which is inversely proportional to the slope height. Fitting results in according to Figure 7b and Table S2, S@VN@NC has the highest slope, indicating the lowest diffusion resistance among all three samples.

S@VN@NC, S@VN/NC and S@NC Li-S cells were further cycled 5 times at 0.1, 0.2, 0.5, 1 and 2 C to evaluate their rate performance, as shown in Figure 7c. The S@VN@NC cell demonstrated stable rate performance at both low and high rates and its discharge capacity returned to the initial value after the current density dropped back to 0.2 C, further proving its excellent reversibility. Obvious discharge voltage platforms were observed in the charge/discharge curves of S@VN@NC at 0.1, 0.2, 0.5, 1 and 2 C, testifying to its excellent electrocatalytic activity and structural stability.[36]

The adsorption capacity of Li_2S_6 on VN@NC, VN/NC and NC was further investigated by measuring the color change 30 min after adding 20 mg of the samples to Li_2S_6 solutions (Figure 8a). Complete discoloration occurred only for VN@NC, demonstrating its highest capacity for polysulfides adsorption.[37] This was further confirmed by UV-vis adsorption spectra displayed in Figure 8b, where the characteristic peak around 425 nm disappeared only for VN@NC containing Li_2S_6 solution. High adsorption capacity of VN@NC mainly results from the effect of VN particles well dispersed on porous N-doped carbon. In the case of VN/NC, the adsorption performance was limited by large and non-uniform VN particles present on the carbon surface. XPS analysis was performed on VN@NC-Li_2S_6, VN/NC-Li_2S_6, and NC-Li_2S_6 samples after the solvent was evaporated in a glove box. According to the fitted S 2p XPS curve, the peaks at 163.0 and 164.1 eV were attributed to the presence of ST^{-1}, the peaks at 163.98 and 165.2 eV represent $S_B{}^0$ and the peaks at 168.03 eV and 169.19 eV correspond to sulfur oxides SO_x, such as thiosulfate, polysulfate and sulfate, which are generally considered as intermediates in polysulfide redox reactions.[38] As shown in Figure 8c, large amount of intermediates was present in VN@NC, confirming its higher polysulfide redox catalytic activity.

Conclusions

Highly dispersed VN on porous N-doped carbon was successfully prepared via one-pot pyrolysis in the molten salt. The method can effectively reduce VN particles aggregation and improve their dispersion on porous N-doped carbon, providing required adsorption sites for sulfur loading and sufficient space for subsequent sulfur volume expansion during the charge/discharge operation of Li–S batteries. When used as a cathode, S@VN@NC demonstrated an initial discharge capacity of 1050 mAh g^{-1} at 0.2 C and maintained the cell capacity at 802 mAh g^{-1} after 100 charge/discharge circles. With an initial discharge capacity of 701 mAh g^{-1}, the Li–S cell exhibited good cycling stability at 1 C with a decay rate of only 0.071% per cycle after 500 cycles. The superior electrocatalytic performance of S@VN@NC in the Li–S cell resulted from the redox process acceleration by VN nanoparticles well dispersed in the porous structure of N-doped carbon, making this newly developed cathode material a promising candidate for the application in Li–S batteries.

Supporting Information Summary

The supporting information includes physical and chemical test conditions. Compare SEM, XRD, thermogravimetry and circulation diagram of different metal content of samples; Performance comparison table and impedance fitting results with current literature

Acknowledgements

The authors would like to thank the Natural Science Foundation of Shandong Province of China (ZR2020MB024) for financially supporting this work.

Conflict of Interest

There are no conflicts to declare.

Data Availability Statement

The data that support the findings of this study are available in the supplementary material of this article.

Keywords: Cathode · 3D Carbon Network · Lithium-sulfur Battery · N-doped carbon · Vanadium Nitride

[1] S. Dai, Y. Feng, P. Wang, H. Wang, H. Liang, R. Wang, V. Linkov, S. Ji, *Electrochim. Acta* **2019**, *321*, 134678.
[2] T. An, D. Deng, M. Lei, Q.-H. Wu, Z. Tian, M. Zheng, Q. Dong, *J. Mater. Chem. A* **2016**, *4*, 12858–12864.
[3] Y. Chen, T. Wang, H. Tian, D. Su, Q. Zhang, G. Wang, *Adv. Mater.* **2021**, *33*, 2003666.
[4] W. Weng, J. Xiao, Y. Shen, X. Liang, T. Lv, W. Xiao, *Angew. Chem. Int. Ed.* **2021**, *60*, 24905–24909.
[5] L. Chai, L. Zhang, X. Wang, L. Xu, C. Han, T.-T. Li, Y. Hu, J. Qian, S. Huang, *Carbon* **2019**, *146*, 248–256.
[6] D. Cheng, Y. Zhao, X. Tang, T. An, X. Wang, H. Zhou, D. Zhang, T. Fan, *Carbon* **2019**, *149*, 750–759.
[7] R. Wang, Z. Chen, Y. Sun, C. Chang, C. Ding, R. Wu, T *Chem. Eng. J.* **2020**, *399*, 125686.
[8] Q. Wu, X. Zhou, J. Xu, F. Cao, C. Li, *ACS Nano* **2019**, *13(8)*, 9520–9532.
[9] Z. Jian, H. Li, R. Cao, H. Zhou, H. Xu, G. Zhao, Y. Xing, S. Zhang, *Electrochim. Acta* **2019**, *319*, 359–365.
[10] S. Tan, Y. Dai, Y. Jiang, Q. Wei, G. Zhang, F. Xiong, X. Zhu, Z. Y. Hu, L. Zhou, Y. Jin, K. Kanamura, Q. An, L. Mai, *Adv. Funct. Mater.* **2020**, *31(7)*, 2008034.
[11] Z. Jiang, Z. Zeng, W. Hu, Z. Han, S. Cheng, J. Xie, *Energy Storage Mater.* **2021**, *36*, 333–340.
[12] D. Cai, Y. Zhuang, B. Fei, C. Zhang, Y. Wang, Q. Chen, H. Zhan, *Chem. Eng. J.* **2022**, *430*, 132931.
[13] L. Niu, Y. Cai, T. Dong, Y. Zhang, X. Liu, X. Zhang, L. Zeng, A. Liu, *Biosens. Bioelectron.* **2022**, *210*, 114285.
[14] L. Xu, W. Guo, L. Zeng, X. Xia, Y. Wang, P. Xiong, Q. Chen, J. Zhang, M. Wei, Q. Qian, *Chem. Eng. J.* **2021**, *419*, 129607.
[15] J. He, A. Manthiram, *Adv. Energy Mater.* **2019**, *10(3)*, 1903241.
[16] C. Ye, Y. Jiao, H. Jin, A. D. Slattery, K. Davey, H. Wang, S. Z. Qiao, *Angew. Chem. Int. Ed.* **2018**, *57(51)*, 16703–16707.
[17] N. Li, Z. Xu, P. Wang, Z. Zhang, B. Hong, J. Li, Y. Lai, *Chem. Eng. J.* **2020**, *398*, 125432.
[18] L. Qiao, L. Ren, R. Zhang, J. Chen, M. Xu, J. Liu, H. Xu, W. Liu, Z. Chang, X. Sun, *Energy Fuels* **2021**, *35(12)*, 10219–10226.
[19] E. Jing, L. Chen, S. Xu, W. Tian, D. Zhang, N. Wang, Z. Bai, X. Zhou, S. Liu, D. Duan, X. Qiu, *J. Energy Chem.* **2022**, *64*, 574–582.
[20] Z. Cheng, Y. Wang, W. Zhang, M. Xu, Boosting *ACS Appl. Energ. Mater.* **2020**, *3(5)*, 4523–4530.
[21] F. Li, M. Zhang, W. Chen, X. Cai, H. Rao, J. Chang, Y. Fang, X. Zhong, Y. Yang, Z. Yang, X. Yu, *ACS Appl. Mater. Interfaces* **2021**, *13(26)*, 30746–30755.
[22] C. X. Zhao, X. Y. Li, M. Zhao, Z. X. Chen, Y. W. Song, W. J. Chen, J. N. Liu, B. Wang, X. Q. Zhang, C. M. Chen, B. Q. Li, J. Q. Huang, Q. Zhang, *J. Am. Chem. Soc.* **2021**, *143(47)*, 19865–19872.
[23] R. Wang, Q. Dong, H. Wang, S. Ji, X. Wang, V. Linkov, *Chem. Eur. J.* **2020**, *26.(47)*, 10752–10758.
[24] Y. Chen, S. Ji, H. Wang, V. Linkov, R. Wang, *Int. J. Hydrogen Energy* **2018**, *43(10)*, 5124–5132.
[25] K. Wan, M.-y. Liu, Z.-p. Yu, Z.-x. Liang, Q.-b. Liu, J.-h. Piao, Y.-y. Zheng, *Int. J. Hydrogen Energy* **2016**, *41(40)*, 18027–18032.
[26] Q. Dong, F. Zhang, S. Ji, X. Wang, H. Wang, V. Linkov, R. Wang, *J. Alloys Compd.* **2021**, *877*, 160286.
[27] Z. Sun, J. Zhang, L. Yin, G. Hu, R. Fang, H. M. Cheng, F. Li, *Nat. Commun.* **2017**, *8*, 14627.
[28] Y. Zhong, D. Chao, S. Deng, J. Zhan, R. Fang, Y. Xia, Y. Wang, X. Wang, X. Xia, J. Tu, *Adv. Funct. Mater.* **2018**, *28(38)*, 1706391.
[29] J. Ding, S. Ji, H. Wang, V. Linkov, R. Wang, *J. Power Sources* **2019**, *423*, 1–8.
[30] J. Ding, S. Ji, H. Wang, V. Linkov, H. Gai, F. Liu, Q. Liu, R. Wang, *ACS Sustainable Chem. Eng.* **2019**, *7*(4), 3974–3981.
[31] H. Y. Zhou, Z. Y. Sui, K. Amin, L. W. Lin, H. Y. Wang, B. H. Han, *ACS Appl. Mater. Interfaces* **2020**, *12*(12), 13904–13913.
[32] L. Xu, X. Chen, W. Guo, L. Zeng, T. Yang, P. Xiong, Q. Chen, J. Zhang, M. Wei, Q. Qian, *Nanoscale* **2021**, *13*(9), 5033–5044.
[33] L. Xu, P. Xiong, L. Zeng, R. Liu, J. Liu, F. Luo, X. Li, Q. Chen, M. Wei, Q. Qian, *Nanoscale* **2020**, *12*(19), 10693–10702.
[34] M. Zhang, L. Wang, B. Wang, B. Zhang, X. Sun, D. Wang, Z. Kong, L. Xu, *J. Mater. Chem. A* **2021**, *9*(10), 6538–6546.
[35] W. Ren, L. Xu, L. Zhu, X. Wang, X. Ma, D. Wang, *ACS Appl. Mater. Interfaces* **2018**, *10*(14), 11642–11651.
[36] Y.-S. Liu, Y.-L. Bai, X. Liu, C. Ma, X.-Y. Wu, X. Wei, Z. Wang, K.-X. Wang, J.-S. Chen, *Chem. Eng. J.* **2019**, *378*, 122208.
[37] X. Lu, Q. Zhang, J. Wang, S. Chen, J. Ge, Z. Liu, L. Wang, H. Ding, D. Gong, H. Yang, X. Yu, J. Zhu, B. Lu, *Chem. Eng. J.* **2019**, *358*, 955–961.
[38] F. Zhang, S. Ji, H. Wang, H. Liang, X. Wang, R. Wang, *Small Methods* **2021**, *5*(6), 2100066.

Submitted: July 24, 2022
Accepted: September 20, 2022